# The mitotic kinesin CENP-E is a processive transport motor

Hasan Yardimci*, Marilyn van Duffelen†, Yinghui Mao‡, Steven S. Rosenfeld†‡§, and Paul R. Selvin*¶‖

*Department of Physics and ¶Center for Biophysics and Computational Biology, University of Illinois at Urbana–Champaign, Urbana, IL 61801; and Departments of †Neurology and ‡Cell Biology and Pathology, Columbia University College of Physicians and Surgeons, New York, NY 10032

*In vivo* studies suggest that centromeric protein E (CENP-E), a kinesin-7 family member, plays a key role in the movement of chromosomes toward the metaphase plate during mitosis. How CENP-E accomplishes this crucial task, however, is not clear. Here we present single-molecule measurements of CENP-E that demonstrate that this motor moves processively toward the plus end of microtubules, with an average run length of $2.6 \pm 0.2$ $\mu$m, in a hand-over-hand fashion, taking 8-nm steps with a stall force of $6 \pm 0.1$ pN. The ATP dependence of motor velocity obeys Michaelis–Menten kinetics with $K_{M,ATP} = 35 \pm 5$ $\mu$M. All of these features are remarkably similar to those for kinesin-1—a highly processive transport motor. We, therefore, propose that CENP-E transports chromosomes in a manner analogous to how kinesin-1 transports cytoplasmic vesicles.

mitotic motor | single molecule

Cell division requires proper attachment of chromosomes to spindle microtubules, which occurs by means of a multiprotein complex called the kinetochore. Centromeric protein E (CENP-E), a kinetochore-associated member of the kinesin superfamily, plays an essential role in capturing and positioning chromosomes to the mitotic spindle during metaphase (1). CENP-E localizes to kinetochores throughout chromosome congression and remains there until anaphase, at which point it relocates to the spindle midzone and is subsequently degraded (2).

Interfering with CENP-E function significantly affects chromosome movement. Injection of an anti-CENP-E antibody leads to mitotic arrest, with either mono-oriented chromosomes positioned close to spindle poles or bi-oriented chromosomes that cannot align on the metaphase plate (1). Depletion of CENP-E from *Xenopus* egg extracts disturbs metaphase chromosome alignment (3), and gene silencing of CENP-E by RNA interference in HeLa cells produces unaligned chromosomes (4). A recent study by Kapoor *et al.* (5) suggests that CENP-E can transport mono-oriented chromosomes to the metaphase plate along the spindle fibers that are attached to already bi-oriented chromosomes. It has further been proposed (6) that CENP-E is responsible for silencing the mitotic checkpoint signaling, through its capture of spindle microtubules at the kinetochore.

These roles for CENP-E represent a diverse set of functions and thus do not provide us with a unifying mechanism to explain how this kinetochore protein functions in mitosis. One approach to addressing this question is to compare the structure of CENP-E with that of other kinesins of known function. However, the crystallographic model of CENP-E resembles that of kinesin-1 (a transport motor) in some respects, and Eg5 (a mitotic motor designed to generate sustained force) in others (7). Previous *in vitro* functional studies of the CENP-E motor also have not been helpful in defining how this kinesin functions physiologically. A study of CENP-E purified from HeLa cells (8) demonstrated that it can bind to microtubules but does not generate microtubule-gliding activity. Another study (9) suggested that CENP-E couples chromosome position to microtubule depolymerizing activity. On the other hand, Wood *et al.* (3) studied microtubule gliding with polarity-marked microtubules

and demonstrated that a recombinant construct containing the motor domain of CENP-E can function as a plus-end-directed motor. Further support for plus-end-directed movement came from studies suggesting that transport of chromosomes toward microtubule plus ends requires CENP-E (5, 10). There thus remains a need to characterize how the CENP-E motor functions because such information may provide insight into how this motor functions physiologically.

Single-molecule techniques have shown that kinesin-1 can transport vesicles and organelles long distances along microtubules and that this motor takes 8-nm steps in an asymmetric, hand-over-hand fashion (11–14). Other studies using single-molecule optical trapping (15) have shown that individual kinesin-1 can produce forces up to 5–7 pN. By contrast, a number of mitotic kinesins, including Eg5, are minimally processive or not processive at all (16–19). Therefore, the approach we have used in this study is to determine whether CENP-E functions like a kinesin-1 transport motor, an Eg5 mitotic motor, or something else altogether.

## Results and Discussion

For single-molecule measurements, we used a leucine-zippered *Xenopus* CENP-E construct consisting of amino acid residues 1–392 fused at the carboxyl terminus to a leucine zipper, followed by a hexahistidine tag for affinity purification. Equilibrium and velocity sedimentation studies revealed that the leucine zipper was required in order to maintain the motor in a dimeric state (M.v.D., J. J. Correia, and S.S.R., unpublished work). The microtubule-activated ATPase activity was characterized by values of $13.5 \pm 0.8$ s$^{-1}$ and $0.35 \pm 0.08$ $\mu$M for $k_{cat}$ and $K_{0.5,MT}$, respectively.

We labeled our dimeric CENP-E construct with quantum dots (20, 21) to visualize individual motor molecules through their movement on microtubules. Streptavidin-conjugated quantum dots were initially functionalized with biotinylated anti-histidine antibody and were then coupled to CENP-E dimers through the hexahistidine tag on their tail region. The position of the quantum dots was monitored by total internal reflection fluorescence (TIRF) microscopy while CENP-E was observed to move on axonemes that were immobilized on a coverslip.
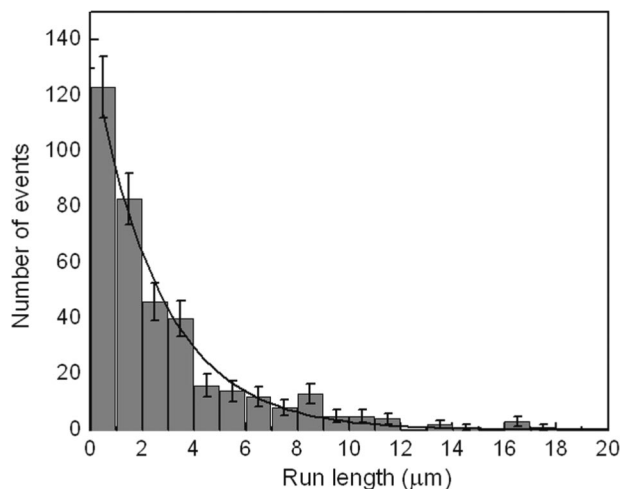
**Fig. 1.** Run length histogram of CENP-E. Run lengths of quantum dot-labeled CENP-E molecules were measured by TIRF microscopy as described in *SI Materials and Methods*. The average run length was determined by fitting a single exponential decay to the histogram. The solid line shows such a fit yielding an average run length of 2.6 ± 0.2 $\mu$m.

Observation of single-molecule characteristics requires ensuring that multiple motors do not attach to the same cargo. For this purpose, we used a CENP-E dimer-to-quantum-dot ratio of 1:4 in our assays (21, 22). At this ratio, we observed that quantum dots traveled long distances [supporting information (SI) Movie S1], implying that individual CENP-E dimers can move processively along microtubules. To quantify this processivity, we measured the run length of our CENP-E dimers at saturating ATP concentrations. The length of individual runs was determined, and a histogram of all runs is plotted in Fig. 1. A single exponential fit with zero offset to the histogram yielded an average run length of 2.6 ± 0.2 $\mu$m. The average run length is comparable to the length of axonemes in our assays. This finding is consistent with our observation that a significant number of motors reached the end of axonemes before detaching. In case the run length was underestimated because of motors that reached the end of axonemes, we measured the run length by using a bead assay in an optical trap. This approach allowed us to adjust the bead position before initiating each run, to ensure that the starting position of the bead was far from the end of axoneme. The mean run length
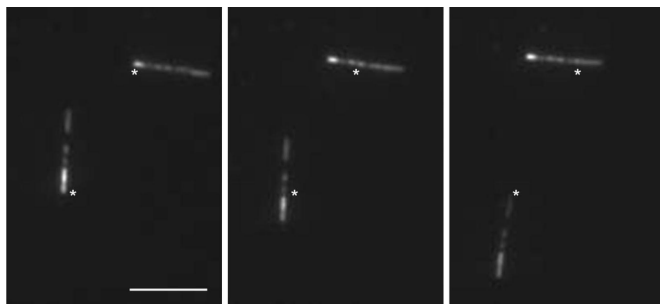


**Fig. 2.** CENP-E-driven gliding of microtubules. Shown are three images from a video sequence (Movie S2) with 12-s intervals between each frame, showing plus-end-directed motility by CENP-E. Rhodamine-labeled microtubule seeds were prepared with a 1:1 ratio of rhodamine tubulin to nonlabeled tubulin. A dilute solution of 1:10 labeled-to-nonlabeled tubulin was added into highly labeled seeds to create microtubules with brighter minus ends. Marks in the images are reference points indicating the initial positions of microtubule minus ends. (Scale bar, 5 $\mu$m.)
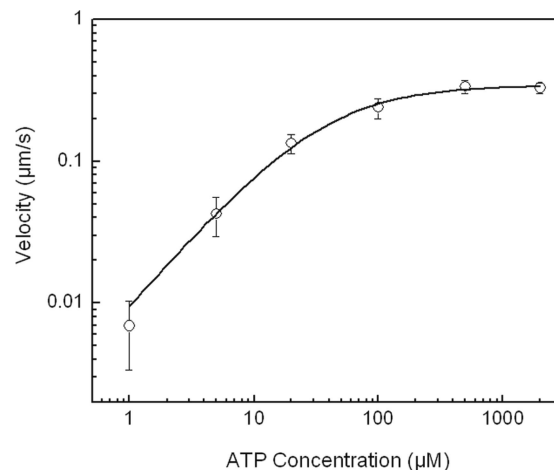


**Fig. 3.** Average velocity of CENP-E as a function of ATP concentration. The solid line is a fit to a Michaelis–Menten equation with $K_M = 35 \pm 5$ $\mu$M and $V_{max} = 342 \pm 10$ nm s$^{-1}$.

measured for CENP-E in this bead assay was 2.4 ± 0.2 $\mu$m. This result confirms the run length measured by using quantum dot-labeled motors. For comparison, we characterized the average distance traveled by a truncated dimeric kinesin-1 construct (K560) with a hexahistidine tag at the carboxyl terminus, using the same bead assay, and measured a run length of 2.7 ± 0.2 $\mu$m. This distance is in agreement with previous studies of kinesin-1 performed under similar conditions (22, 23). In addition, similar to kinesin-1 (24), beads traveled longer distances when a high concentration of CENP-E motors was used. This indicates that multiple motors enhance cargo transport.

To assess the directionality of CENP-E, we performed microtubule gliding assays with polarity-marked microtubules in which the minus ends were heavily fluorescently labeled. This method has previously been used to study the directionality of other members of the kinesin superfamily (25, 26). In this assay, microtubules moved with their minus ends leading, as illustrated in Fig. 2 and Movie S2, indicating that CENP-E
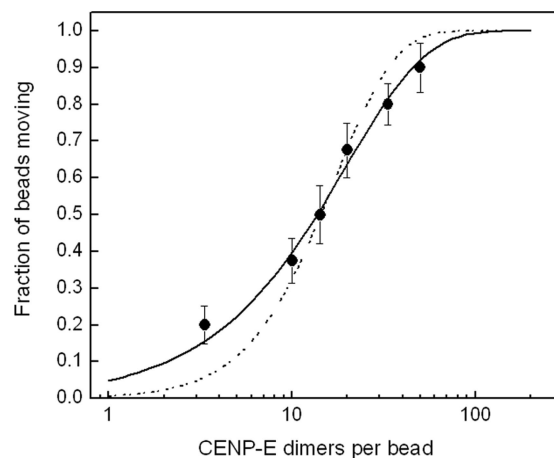


**Fig. 4.** Fraction of beads moving vs. CENP-E-to-bead ratio. The beads were brought into contact with axonemes for >30 s. In most cases, more than two axonemes were tried if no motility was observed. Measurement at each concentration includes 20–60 beads. The solid line is a fit to single exponential $1 - \exp(-\lambda c)$, where $c$ is the CENP-E-to-bead ratio representing beads carried by one motor. The data cannot be fit well if more than one motor is assumed to be required for motility, $1 - \exp(-\lambda c) - \lambda c \exp(\lambda c)$ (dashed line).

**Fig. 5.** Stall force measurements of CENP-E. (*a*) Sample trace of bead displacement by CENP-E in a static laser trap, displaying seven runs, each followed by a rapid detachment at high loads. The measurement was done at saturati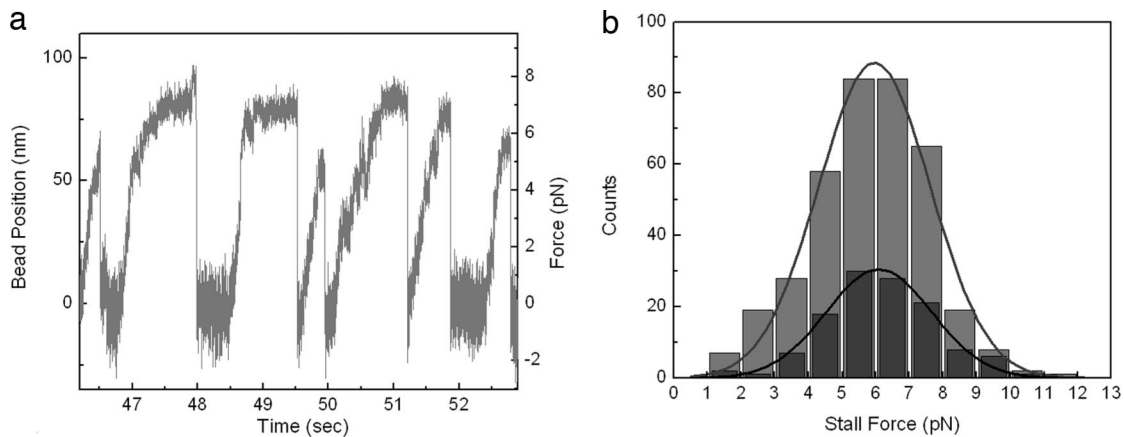ng ATP concentrations. The trap stiffness was 0.086 pN/nm, and the data collection rate was 3 kHz. (*b*) Stall force distributions of CENP-E (light gray) and K560 (dark gray). The lines are fits to a Gaussian function. The average stall forces are 5.96 ± 0.08 pN (*n* = 375) for CENP-E and 6.09 ± 0.08 pN (*n* = 122) for K560. Stall events that lasted <50 ms at the highest force were not included.

is a plus-end-directed motor. This result is in agreement with an earlier study (3). In addition, we verified plus-end-directed movement of quantum dot-labeled CENP-E motors in single-molecule experiments by comparing the travel direction of CENP-E with that of K560 in the same assay. This was achieved by removing quantum dot-labeled CENP-E motors by washing the sample chamber and introducing K560 mole-

cules without significantly moving the chamber. Indeed, the K560 molecules moved in the same direction (data not shown).

To characterize the kinetics of ATP binding and catalysis, the speed of the motors was studied as a function of ATP concentration. Fig. 3 illustrates the ATP dependence of the speed from an average of at least 15 individual runs at each ATP concentration.
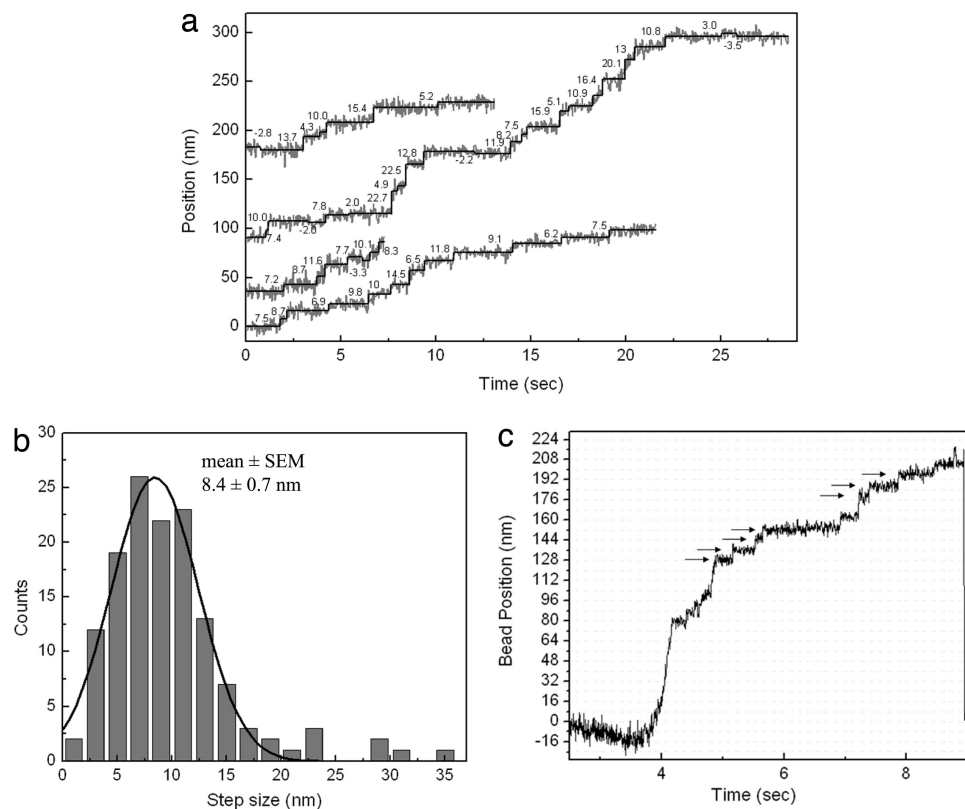


**Fig. 6.** Stepping mechanism of CENP-E dimers by FIONA. (*a*) Sample traces of position vs. time for CENP-E motors labeled with a quantum dot at the tail displaying the center of mass displacement. Values near traces show individual step sizes in nanometers. Measurements were done at 1 μM ATP, and an image was acquired every 30 ms. (*b*) Step-size histogram of CENP-E. Gaussian fit (solid line) to the histogram returned an average step size of 8.4 ± 0.7 nm. Large steps (20–40 nm) in the histogram are believed to be due to multiple steps or fast diffusive motion of motors. (*c*) Bead displacement in a fixed trap while carried by CENP-E at 10 μM ATP and at 0.25 kHz data collection rate. Position of the bead was determined by bright-field imaging with one-nanometer accuracy (bFIONA) (38) and shows clear step-wise motion. Arrows indicate positions of ≈8-nm steps.
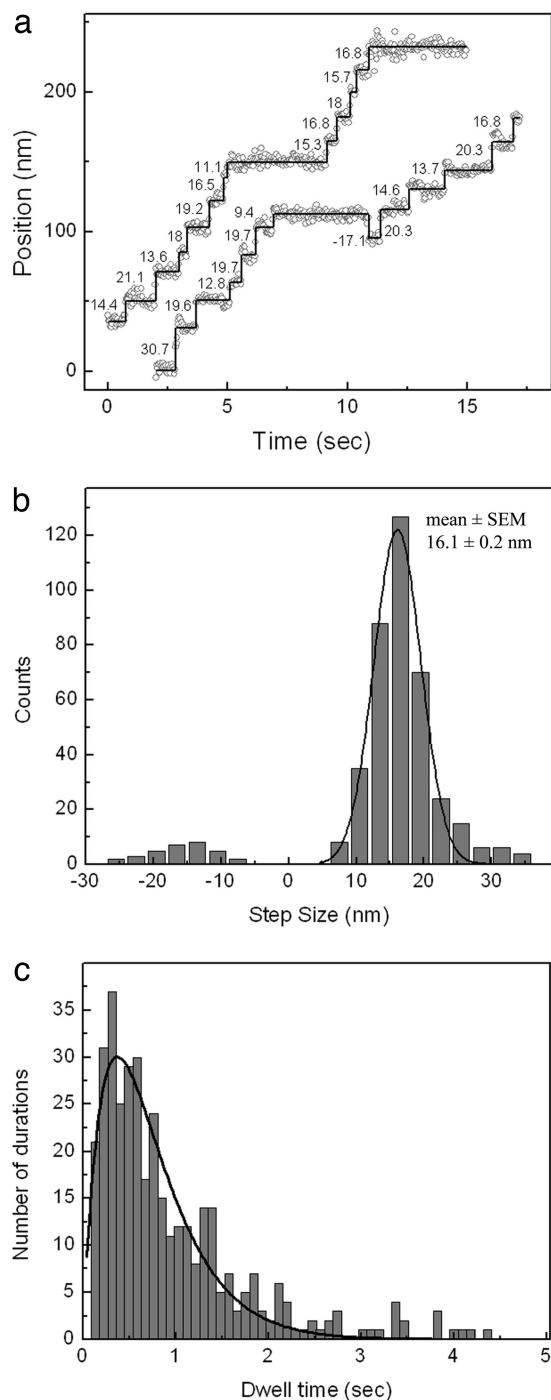
**Fig. 7.** Hand-over-hand movement of CENP-E. (*a*) Sample traces of position vs. time for CENP-E motors labeled on motor domain with quantum dot. Values near traces show individual step sizes in nanometers. Measurements were done at 2 $\mu$M ATP, and an image was acquired every 30 ms. (*b*) Step-size histogram of head-labeled CENP-E. Gaussian fit (solid line) to the histogram returned an average step size of 16.1 ± 0.2 nm. Average step size in the backward direction is ≈15 nm. (*c*) Dwell-time histogram of steps from head-labeled CENP-E motors. The solid line is a fit to $Atk^2 \exp(-kt)$, which returned a rate constant $k = 2.68 \pm 0.1$ s$^{-1}$.

The data fit a Michaelis–Menten equation with Michaelis constant $K_{M,ATP} = 35 \pm 5$ $\mu$M, in agreement with steady-state solution kinetics ($K_{M,ATP} = 42 \pm 9$ $\mu$M). Similar values for $K_{M,ATP}$ of kinesin-1 are reported in both single-molecule (27) and steady-state ATPase measurements (28).

We investigated the amount of force produced by single CENP-E motors through the use of an optical trap (19, 29, 30). Motors were coupled to streptavidin-coated polystyrene beads by using a conjugation method similar to that used for the quantum dots. Beads were trapped by an infrared laser beam and held near an axoneme that was immobilized on the surface. To examine whether one CENP-E dimer is sufficient to transport a bead on a microtubule, the ratio of beads capable of moving when brought into contact with an axoneme was determined as a function of motor concentration, as illustrated in Fig. 4. The data fit to a single exponential, confirming that one motor is adequate to move a bead (31).

We next determined the maximum force generated by an individual CENP-E motor by studying the motility of trapped beads. In a stationary trap, a motor that attaches to an axoneme and moves processively in one direction feels greater force with displacement opposite to the direction of movement. After moving a distance, the motor stalls, detaches from axoneme, and is pulled back to the trap center, where it can bind and move again (see Movie S3). A sample trace of a series of such events is displayed in Fig. 5*a*. To make a quantitative characterization of the force generated by single motors, we generated a histogram of such stall events and measured an average stall force of 5.96 ± 0.08 pN (Fig. 5*b*). For direct comparison, we also made stall force measurements on our dimeric kinesin-1 construct (K560). Fig. 5*b* displays this comparison and shows that the average stall force of CENP-E is essentially the same as that of K560 (6.09 ± 0.08 pN).

We examined the movement of quantum dot-labeled CENP-E dimers at a low ATP concentration and higher time resolution to differentiate individual steps as molecules move on axonemes. We used fluorescence imaging with one-nanometer accuracy (FIONA) (32), which is capable of determining the position of a single fluorescent spot with nanometer precision. Sample traces of such measurements are plotted in Fig. 6*a* and display step-wise motion. Individual steps were evaluated with a Student *t* test fitting. The resulting distribution of all steps, shown in Fig. 6*b*, gives an average step size of 8.4 ± 0.7 nm, which is essentially the same as for kinesin-1 (13) and is consistent with the distance between tubulin heterodimers along a microtubule protofilament. We also detected step-wise movement in optical trap measurements at limiting ATP concentrations as the beads were carried by motors (Fig. 6*c*). Steps became visible at higher loads as the motor slowed down and Brownian motion of the bead was reduced. We observed that at near-stalling loads, CENP-E occasionally exhibited backward steps, as is seen in kinesin-1 (data not shown).

Two models have been proposed to explain the stepping mechanism of molecular motors: "inchworm" and "hand-over-hand" (12, 14). Both models predict that two identical head domains are coordinated in such a way that one head is always attached to the track. The inchworm model suggests that one of the heads is always in the leading position. This means that, with each step, the leading head moves 8 nm, which is the same size as the movement of the center of mass (12, 14). In contrast, in the hand-over-hand mechanism, the trailing head moves past the leading head with a step size twice that of the stalk. A number of motor proteins, including kinesin-1 (14) and myosin V (32), have been shown to move in a hand-over-hand manner. To test whether CENP-E moves by a hand-over-hand mechanism, we used an amino-terminal, hexahistidine-tagged CENP-E dimeric construct. We labeled the amino termini of this CENP-E construct with quantum dots that were directly conjugated with anti-hexahistidine antibody. Quantum dots attached to the CENP-E amino-terminal motor domains were visualized through TIRF microscopy, and their positions were determined by FIONA. Position traces of the molecules showed clear step-wise movement, as displayed in Fig. 7*a*. We scored a total of 424 steps from 32 molecules. Some traces also showed backward

steps, which make up ≈8% of the total. A histogram of step sizes yielded an average of 16.1 ± 0.2 nm in the forward direction (Fig. 7$b$). This value is approximately twice the step size of the stalk, and thus our results strongly suggest that CENP-E moves in a hand-over-hand fashion, like kinesin-1. In addition, we performed dwell-time analysis of the steps to show that each 16-nm step alternates with a hidden 0-nm step. We interpret the latter to be due to a step by the unlabeled head. If the stepping rates of both heads were the same, the resulting convolution of two exponential decays would give a dwell-time probability that would change as $P(t) = tk^2 \exp(-kt)$ (32), where $k$ is the stepping rate constant. The dwell-time distribution, plotted in Fig. 7$c$, is well fit by this convolution function and not by a single-exponential decay. It yields a rate constant $k = 2.68 ± 0.1$ steps per second, which is consistent with the average velocity determined from these measurements ($v = 19.9 ± 1.4$ nm s$^{-1}$). Therefore, the dwell-time measurements also suggest a hand-over-hand mechanism.

Despite the key roles CENP-E plays in chromosome movement, there has heretofore been no mechanistic information on how this kinesin actually functions. Likewise, comparisons of primary, secondary, and tertiary structures between CENP-E and other kinesin motors—such as kinesin-1 and Eg5—have not been helpful in providing further mechanistic insights. CENP-E is 38% identical to kinesin-1 and 36.1% identical to Eg5 in primary structure. Consequently, there is very little difference in amino acid sequence between CENP-E and these other two motors. Furthermore, the root-mean-square deviation of the Cα atoms of CENP-E and kinesin-1 is 1.1 Å, whereas the corresponding value for CENP-E and Eg5 is 1.5 Å (7). This implies that the peptide backbone has nearly the same three-dimensional orientation for the three motors. These results strongly imply that comparison of structures does not provide insight into function.

As a result, we undertook a detailed mechanistic study of the CENP-E motor at the single-molecule level to see whether its behavior could allow us to propose supportable conclusions about how it functions in the cell as a mitotic motor. Our results clearly show that, although CENP-E is structurally similar to other mitotic kinesins such as Eg5, its enzymatic and mechanical functions more closely resemble those of transport kinesins such as kinesin-1. Our results are entirely consistent with the proposal that CENP-E functions *in vivo* as a motor that carries chromosomes toward the metaphase plate, in a manner very similar to how kinesin-1 transports vesicles. This conclusion is supported by five key findings. First, the average run length for CENP-E is comparable to the distance that chromosomes are observed to move toward the midzone during metaphase oscillation (≈3–4 μm, ref. 5). Second, the Michaelis–Menten dependence of CENP-E velocity on ATP concentration is nearly identical to that for kinesin-1. Third, the average step size of CENP-E, as measured with FIONA, is 8.4-nm—nearly identical to that for kinesin-1. Fourth, the movement of CENP-E, like that for kinesin-1, can be described by a hand-over-hand stepping mechanism. Finally, the force dependence of CENP-E through the optical trap is comparable to that of kinesin-1. Thus, we demonstrate that biophysical measurements of CENP-E at the single-molecule level provide key insights into its cellular physiology.

During metaphase, mono-oriented chromosomes oscillate between the pole and the midzone before aligning at the metaphase plate (5). Forces contributing to poleward-directed motion are believed to be due to microtubule depolymerization (33) and cytoplasmic dynein (34), a minus-end-directed microtubule mo-

lecular motor. Our *in vitro* optical trap measurements demonstrate that CENP-E can produce forces in the opposite direction to those produced by microtubule depolymerization and dynein, and they support models that propose that CENP-E pulls mono-oriented chromosomes toward the midzone and away from the poles (3, 5, 10).

## Materials and Methods

**Steady-State ATPase.** The ATPase rate was determined with the EnzChek phosphate assay kit (Molecular Probes), using a Varian Cary 300 Bio UV-visible spectrophotometer and the Cary kinetics software. The reaction conditions were 100 nM CENP-E monomer, 2 mM ATP, 0.1–12 μM tubulin in ATPase buffer (25 mM Hepes, 100 mM KCl, 2 mM MgCl₂, 1 mM EGTA, 1 mM DTT, pH 7.5).

**Single-Molecule Motility Assays with Quantum Dot-Labeled CENP-E.** Sample flow chambers were prepared by using plasma-cleaned slides and double sticky tape (35). Streptavidin-conjugated quantum dots (Qdot 655; Invitrogen) were mixed with biotinylated penta-His antibody (Qiagen) in BRB10 (10 mM Pipes, 5 mM MgCl₂, 1 mM EGTA) with 2 mM DTT and incubated for 30 min. His-tagged CENP-E was added into this mix at a concentration of 1 CENP-E dimer to 4 quantum dots, to prevent multiple motor attachment to quantum dots. After 1-h incubation, quantum dot-labeled motors were diluted ×100 in motility buffer consisting of BRB10 with 2 mM DTT, 0.2 mg/ml casein, 1% 2-mercaptoethanol, and the desired concentration of MgATP. An ATP regenerating system (1 mM creatine phosphate, 1 unit per milliliter creatine kinase) was also included in this buffer unless saturating ATP was present. All incubations were made on ice.

Axonemes extracted from sea urchin sperm flagella (36) were flowed through the chamber after ×10 dilution in BRB10 and were allowed to attach to the glass surface for 5 min at 4°C. The chamber was washed with BRB10, followed by 15-min incubation with 4 mg/ml casein solution to avoid nonspecific attachment of quantum dots to the glass surface. Finally, the motility buffer with quantum dot-labeled protein was introduced into the chamber.

For measurements with amino-terminal His-tagged CENP-E, dilute concentrations (0.6 nM) of unlabeled CENP-E dimers were initially introduced into the sample chamber and were allowed to attach axonemes for 10 min. Excess protein was washed out, and quantum dots were added at a concentration of ≈1.6 nM. After 10-min incubation, the chamber was washed with motility buffer.

**Gliding Assays with Polarity-Marked Microtubules.** Polarity-marked fluorescent microtubules were prepared as described by Hyman (37), using rhodamine-labeled and unlabeled bovine brain tubulin (Cytoskeleton). The flow chamber was first washed with 4 mg/ml casein in BRB10. CENP-E was added, excess motors were removed, and microtubules were introduced in motility buffer with 20 μM taxol and an oxygen scavenging system containing 4.5 mg/ml glucose, 200 μg/ml glucose oxidase (Sigma–Aldrich), and 35 μg/ml catalase (Roche Diagnostics).

**Bead Assays for Optical Trapping.** Streptavidin-conjugated 0.44-μm-diameter polystyrene beads (Spherotech) were coated with biotinylated anti-His antibody (AbD; Serotec) through 30-min incubation on ice. To remove excess antibody, the bead solution was centrifuged and resuspended twice in BRB10, with 8 mg/ml BSA included as a blocking protein. CENP-E was diluted and mixed with beads in BRB10 containing 8 mg/ml BSA, 2 mM DTT, and 10 μM ATP and incubated for 3 h on ice. Finally, CENP-E-coated beads were introduced into the flow chamber in BRB10 including 2 mM DTT, 2 mM MgATP, and an oxygen scavenging system. Before each incubation step, beads were sonicated for 1–3 min to break aggregates. To ensure that records were from single CENP-E molecules, the concentration of motors was chosen such that fewer than half of the beads moved when brought into contact with an axoneme for at least 30 s.

1. Schaar BT, Chan GKT, Maddox P, Salmon ED, Yen TJ (1997) CENP-E function at kinetochores is essential for chromosome alignment. *J Cell Biol* 139:1373–1382.
2. Yen TJ, Li G, Schaar BT, Szilak I, Cleveland DW (1992) CENP-E is a putative kinetochore motor that accumulates just before mitosis. *Nature* 359:536–539.
3. Wood KW, Sakowicz R, Goldstein LSB, Cleveland DW (1997) CENP-E is a plus end-directed kinetochore motor required for metaphase chromosome alignment. *Cell* 91:357–366.
4. Tanudji M, *et al.* (2004) Gene silencing of CENP-E by small interfering RNA in HeLa cells leads to missegregation of chromosomes after a mitotic delay. *Mol Biol Cell* 15:3771–3781.

Yardimci *et al.*

5. Kapoor TM, *et al.* (2006) Chromosomes can congress to the metaphase plate before biorientation. *Science* 311:388–391.

6. Mao Y, Desai A, Cleveland DW (2005) Microtubule capture by CENP-E silences BubR1-dependent mitotic checkpoint signaling. *J Cell Biol* 170:873–880.

7. Garcia-Saez I, Yen T, Wade RH, Kozielski F (2004) Crystal structure of the motor domain of the human kinetochore protein CENP-E. *J Mol Biol* 340:1107–1116.

8. DeLuca JG, Newton CN, Himes RH, Jordan MA, Wilson L (2001) Purification and characterization of native conventional kinesin, HSET, and CENP-E from mitotic HeLa cells. *J Biol Chem* 276:28014–28021.

9. Lombillo VA, Nislow C, Yen TJ, Gelfand VI, McIntosh JR (1995) Antibodies to the kinesin motor domain and CENP-E inhibit microtubule depolymerization-dependent motion of chromosomes *in vitro*. *J Cell Biol* 128:107–115.

10. Yao X, Anderson KL, Cleveland DW (1997) The microtubule-dependent motor centromere-associated protein E (CENP-E) is an integral component of kinetochore corona fibers that link centromeres to spindle microtubules. *J Cell Biol* 139:435–447.

11. Asbury CL, Fehr AN, Block SM (2003) Kinesin moves by an asymmetric hand-over-hand mechanism. *Science* 302:2130–2134.

12. Hua W, Chung J, Gelles J (2002) Distinguishing inchworm and hand-over-hand processive kinesin movement by neck rotation measurements. *Science* 295:844–848.

13. Svoboda K, Schmidt CF, Schnapp BJ, Block SM (1993) Direct observation of kinesin stepping by optical trapping interferometry. *Nature* 365:721–727.

14. Yildiz A, Tomishige M, Vale RD, Selvin PR (2004) Kinesin walks hand-over-hand. *Science* 303:676–678.

15. Visscher K, Schnitzer MJ, Block SM (1999) Single kinesin molecules studied with a molecular force clamp. *Nature* 400:184–189.

16. Crevel IM-TC, Lockhart A, Cross RA (1997) Kinetic evidence for low chemical processivity in ncd and Eg5. *J Mol Biol* 273:160–170.

17. Rogers KR, *et al.* (2001) KIF1D is a fast non-processive kinesin that demonstrates novel K-loop-dependent mechanochemistry. *EMBO J* 20:5101–5113.

18. Stewart RJ, Semerjian J, Schmidt CF (1998) Highly processive motility is not a general feature of the kinesins. *Eur Biophys J* 27:353–360.

19. Valentine MT, Fordyce PM, Krzysiak TC, Gilbert SP, Block SM (2006) Individual dimers of the mitotic kinesin motor Eg5 step processively and support substantial loads *in vitro*. *Nat Cell Biol* 8:470–476.

20. Courty S, Luccardini C, Bellaiche Y, Cappello G, Dahan M (2006) Tracking individual kinesin motors in living cells using single quantum-dot imaging. *Nano Lett* 6:1491–1495.

21. Seitz A, Surrey T (2006) Processive movement of single kinesins on crowded microtubules visualized using quantum dots. *EMBO J* 25:267–277.

22. Muthukrishnan G, Hutchins BM, Williams ME, Hancock WO (2006) Transport of semiconductor nanocrystals by kinesin molecular motors. *Small* 2:626–630.

23. Vugmeyster Y, Berliner E, Gelles J (1998) Release of isolated single kinesin molecules from microtubules. *Biochemistry* 37:747–757.

24. Block SM, Goldstein LSB, Schnapp BJ (1990) Bead movement by single kinesin molecules studied with optical tweezers. *Nature* 348:348–352.

25. Sawin KE, LeGuellec K, Philippe M, Mitchison TJ (1992) Mitotic spindle organization by a plus-end-directed microtubule motor. *Nature* 359:540–543.

26. Stewart RJ, Thaler JP, Goldstein LSB (1993) Direction of microtubule movement is an intrinsic property of the motor domains of kinesin heavy chain and *Drosophila* ncd protein. *Proc Natl Acad Sci USA* 90:5209–5213.

27. Nishiyama M, Higuchi H, Yanagida T (2002) Chemomechanical coupling of the forward and backward steps of single kinesin molecules. *Nat Cell Biol* 4:790–797.

28. Gilbert SP, Johnson KA (1993) Expression, purification, and characterization of the *Drosophila* kinesin motor domain produced in *Escherichia coli*. *Biochemistry* 32:4677–4684.

29. Mehta AD, *et al.* (1999) Myosin-V is a processive actin-based motor. *Nature* 400:590–593.

30. Toba S, Watanabe TM, Yamaguchi-Okimoto L, Toyoshima YY, Higuchi H (2006) Overlapping hand-over-hand mechanism of single molecular motility of cytoplasmic dynein. *Proc Natl Acad Sci USA* 103:5741–5745.

31. Svoboda K, Block SM (1994) Force and velocity measured for single kinesin molecules. *Cell* 77:773–784.

32. Yildiz A, *et al.* (2003) Myosin V walks hand-over-hand: Single fluorophore imaging with 1.5-nm localization. *Science* 300:2061–2065.

33. Grishchuk EL, McIntosh JR (2006) Microtubule depolymerization can drive poleward chromosome motion in fission yeast. *EMBO J* 25:4888–4896.

34. Sharp DJ, Rogers GC, Scholey JM (2000) Cytoplasmic dynein is required for poleward chromosome movement during mitosis in *Drosophila* embryos. *Nat Cell Biol* 2:922–930.

35. Selvin PR, *et al.* (2007) *In vitro* and *in vivo* FIONA and other acronyms for watching molecular motors walk. *Single-Molecule Techniques: A Laboratory Manual*, eds Selvin PR, Ha T (Cold Spring Harbor Press, Cold Spring Harbor, NY), pp 37–71.

36. Gibbons IR, Fronk E (1979) A latent adenosine triphosphatase form of dynein 1 from sea urchin sperm flagella. *J Biol Chem* 254:187–196.

37. Hyman AA (1991). Preparation of marked microtubules for the assay of the polarity of microtubule-based motors by fluorescence. *J Cell Sci* 14(Suppl):125–127.

38. Kural C, *et al.* (2007) Tracking melanosomes inside a cell to study molecular motors and their interaction. *Proc Natl Acad Sci USA* 104:5378–5382.

**BIOPHYSICS**